JOURNAL OF GEOPHYSICAL RESEARCH, VOL. 93, NO. B2, PAGES 1087–1102, FEBRUARY 10, 1988

Origin of Reflections From the Brevard Fault Zone

NIKOLAS I. CHRISTENSEN AND DANIEL L. SZYMANSKI

Department of Earth and Atmospheric Sciences, Purdue University, West Lafayette, Indiana

The Brevard fault zone is a belt of mylonitic metamorphic rocks that extends northeast over 700 km from Alabama into Virginia. Seismic reflection studies show that the fault zone produces excellent reflections which dip gently to the southeast and sole at depth. The origin of these reflections has been investigated by measuring compressional wave velocities to 800 MPa confining pressure in 127 samples obtained from drill core which continuously sampled the fault zone to a depth of over 300 m. Densities are reported as well as chemical analyses at selected depths. Anisotropy at elevated pressures ranges within the fault zone from less than 5% to over 26%. Similarly, the fault zone rocks show significant chemical variability, with SiO_2 ranging from 58.0 to 70.4% by weight. Synthetic seismograms generated from the velocity and density measurements show that the reflections originate within the Brevard fault zone from the complex interaction of compositional variations and seismic anisotropy resulting from ductile strain. Essential to this study has been the continuous coring of a major section of the Brevard fault zone, which has provided the necessary stratigraphic control as well as unweathered samples for laboratory studies.

INTRODUCTION

Seismic reflection profiling, a technique once used almost exclusively for hydrocarbon exploration in sedimentary terranes, is now being used to image all levels of the crystalline continental crust. Lower crustal reflections including reflections originating near the Moho are often attributed to laterally discontinuous horizontal laminations [e.g., *Meissner*, 1973; *Phinney and Jurdy*, 1979; *Hale and Thompson*, 1982; *Matthews and Cheadle*, 1986] possibly produced by ductile extension. Strong, gently dipping reflections in the upper crystalline crust have been traced to surface exposures of mylonite zones [e.g., *Brewer et al.*, 1983; *Hurich et al.*, 1985]. An understanding of the origins of these reflections has clearly lagged behind field observations.

In this paper we investigate the origin of reflections from a major continental thrust/strike-slip fault. The Brevard fault appears on seismic reflection records as a zone of gently dipping reflectors which sole at depth [*Clark et al.*, 1978; *Cook et al.*, 1979, 1983; *Harris et al.*, 1981; *Williams et al.*, 1987; *Coruh et al.*, 1987]. Speculations on the origin of reflections from this fault zone have been poorly constrained due, in part, to inadequate velocity information on Brevard fault zone lithologies. Because of weathering, rocks from the limited surface exposures of the Brevard zone are usually unsatisfactory for laboratory velocity measurements. Fortunately, however, a recent test hole drilled into the Brevard fault zone to a depth of 330 m recovered a complete suite of unaltered samples for velocity, density, petrographic, and chemical analyses. The results of this study provide insight into the origin of reflections from the Brevard fault zone and perhaps other major fault zones in crystalline terranes throughout the world.

BREVARD FAULT ZONE

The Brevard fault zone is a 0.5- to 3.0-km-wide belt of mylonitic and low-grade metamorphic rocks extending at least 725 km northeastward from central Alabama into Virginia (Figure 1). This remarkably linear feature is a major structural element of the southern Appalachians, forming the boundary between two crystalline terranes: the Blue Ridge to the northwest and the Piedmont to the southeast. The Brevard fault zone coincides for much of its length with a marked elevation difference between the Blue Ridge and the topographically lower Piedmont. The zone loses its linear character at its southwest end, where it appears to splay.

The most distinguishing characteristic of the Brevard fault zone is the preponderance of phyllonites, mylonites, and mylonitic gneisses which were apparently derived from metasedimentary units and gneisses. These lithologies were first described in detail by *Keith* [1905] near Brevard, North Carolina. The rocks in the zone experienced at least one garnet-amphibolite grade metamorphic event but were subsequently retrograded to greenschist facies assemblages. Foliation within the zone generally dips moderately to the southeast but can be locally vertical. The variation in dip influences the surface width of the zone, but *Hatcher* [1968] estimated the true thickness of the Brevard fault zone at 0.5–0.6 km near the surface.

Concentrating on the stratigraphy of the Brevard fault zone rocks, *Hatcher* [1968, 1970, 1971] observed that a very similar sequence of lithologies parallels the Brevard fault zone from central Georgia to east of Asheville, North Carolina. These units are part of the Chauga belt synform. The Brevard fault zone apparently developed within incompetent phyllites of the Chauga River Formation along the northwest limb of this synform. Northeast of Asheville the fault zone occurs in unnamed metasedimentary rocks [*Hatcher*, 1975]. These observations suggest that the location of the Brevard fault zone may be lithologically controlled. However, the prevalence of cataclastic and mylonitic textures within the zone indicates that the deformation in the zone has affected the lithology.

Limited exposure of unweathered rock, coupled with a complex tectonic and metamorphic history and, until recently, lack of subsurface information, has led to many interpretations for the origin and tectonic significance of the Brevard fault zone. *Hatcher* [1971, 1975] revived and synthesized several existing models when he interpreted the Brevard fault zone as a major northwest directed thrust

Paper number 7B6036.
0148-0227/88/007B-6036$05.00

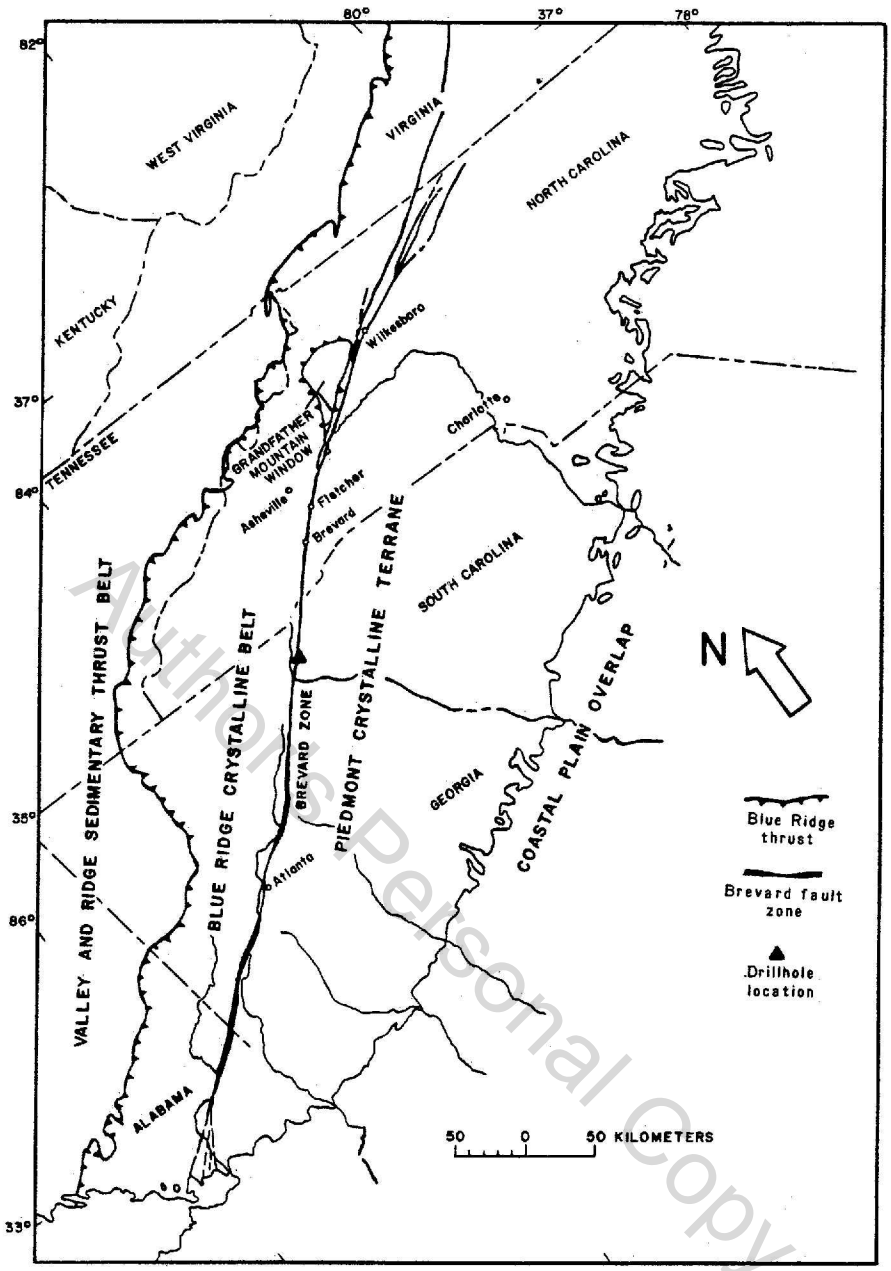

Fig. 1. Map showing the location of the Brevard fault zone.

[after *Jonas*, 1932] with perhaps a minor strike-slip component [after *Reed et al.*, 1970] localized along the northwest limb of a Piedmont synclinorium [after *Keith*, 1905]. In support of the thrust fault model, *Hatcher* [1971] cited the repetition of stratigraphic units within the zone, "exotic" slices of carbonates and basement material presumably plucked off the footwall during thrusting, and truncation of lithologic units by the fault.

Hatcher [1978] envisioned the Brevard fault zone as the ductile root in which a family of Blue Ridge thrusts developed. The fault zone was reactivated several times subsequently, and during the Alleghanian a brittle backlimb thrust formed and broke free from the Blue Ridge root zone. This is the exposure of the Brevard fault zone seen on the surface today.

The subsurface geometry of the Brevard fault zone reflectors seen on reflection profiles agrees with a thrust fault interpretation. *Clark et al.* [1978] described two seismic reflection surveys conducted just southeast of the Brevard fault zone, which yielded two profiles 1 km and 0.6 km in length. On these profiles, Clark et al. recognized two strong reflectors, which they interpreted as the top and base of the Brevard fault zone, giving the zone a thickness of approximately 0.3 s of two-way travel time (~0.9 km). The Henderson Gneiss overlies the zone, while Precambrian metasedimentary rocks, Grenville-age basement, or Cambrian platform strata are interpreted to underlie the zone. Reflections between the interpreted top and base of the zone show variable dip; the strongest of these internal reflections were believed by Clark et al. to represent multiples or out-of-plane diffractions.

The Consortium for Continental Reflection Profiling (COCORP) [*Cook et al.*, 1979, 1983] conducted the first part of their southern Appalachian traverse across the Brevard

fault zone. They imaged to much greater depths than Clark et al.; consequently, their profiles do not record subtle features in the upper crust. The Brevard fault zone appears on COCORP records as a rather incoherent package of reflectors (~0.6 km thick) which apparently soles at a depth of ~9 km, merging with a series of strong, horizontal, layered reflectors approximately 1 km thick.

Most recently, seismic reflection profiles, collected by the Appalachian Ultradeep Corehole Project study group (ADCOH), show the Brevard fault zone to be characterized by at least one relatively continuous, high-amplitude reflection which parallels, but does not merge with, the thick zone of reflectors also seen on the COCORP profile (Figure 2). Similar relationships are visible, though less distinctly, on the U.S. Geological Survey (USGS) seismic lines of *Harris et al.* [1981]. *Hatcher et al.* [1987] interpreted the Brevard fault zone imaged on ADCOH records as an essentially knife edge fault at depth which splays brittlely near the surface to produce its 0.5- to 3.0-km-wide surface exposure pattern. However, we interpret the seismic data to indicate that the surface thickness of the Brevard fault zone is maintained, or perhaps increases, with depth. An increase in amplitude of Brevard zone reflections at depth may be due to decreasing dip of foliation and to granitic gneiss and amphibolite of the Piedmont terrane being ductilely sheared in the fault zone.

PHYSICAL AND CHEMICAL PROPERTIES OF BREVARD FAULT ZONE MYLONITES

In 1985 the National Science Foundation sponsored a site investigation of an 8600 km^2 area in the southern Appalachians [*Williams et al.*, 1987]. The purpose of this study was to explore the possibility of drilling a 10- to 11-km-deep hole through several major crystalline thrust sheets into the autochthonous North American basement and its deformed Paleozoic platform sedimentary rocks [*Hatcher*, 1987]. This project included surface geologic mapping, seismic reflection studies, and shallow drilling.

The four drill holes shown in Figure 3 were selected to provide information on the drilling characteristics of the different crystalline terranes in the area and to allow standard logging experiments to be performed in the holes. Of particular importance, one hole (DH-2) was located within the Brevard fault zone. Drilling at this site penetrated 330 m of fault zone rock with nearly 100% recovery. Because of its continuity and, with the exception of the upper 15 m, its unweathered nature the drill core provided a unique opportunity to study the origin of seismic reflections from a major fault zone.

The rocks from the Brevard drill core are micaceous quartzofeldspathic mylonitic gneisses and schists. Variable amounts of garnet, chlorite, epidote, and carbonate are present. Neomineralization and recrystallization are dominant over cataclastic features (Figure 4). The present mineralogy is suggestive of conditions transitional between the greenschist and amphibolite facies. However, this is complicated by a polymetamorphic origin of the mylonites. The lithologies have been subject to both prograde and retrograde metamorphic processes followed by brittle deformation [*Hatcher*, 1970; *Roper and Justus*, 1973]. Foliations in the core vary in dip from 15° to 30° and generally dip about 20°.

Chemical analyses of selected samples from the Brevard drill core are presented in Table 1 along with estimates of the average chemical composition of shale and granite. Several samples from the upper portion of the hole are similar in chemistry to shale. A sedimentary origin for these rocks is thus likely. This is also supported by the presence of graphite and carbonates in some Brevard fault zone rocks [*Hatcher*, 1970; *Roper and Justus*, 1973]. The mylonites from the lower portion of the hole, which were likely derived from Henderson Gneiss, are chemically similar to granite.

Petrologic core descriptions were used to select representative samples at closely spaced intervals. Thirty-four samples were selected from the Brevard fault zone core with an average spacing of 9.25 m. From these samples, 127 minicores, 2.5 cm in diameter and 4–6 cm in length, were cored and trimmed for velocity measurements as a function of pressure. To investigate seismic anisotropy, four cores, designated A, B, C, and D, were taken from each sample. The axes of the A cores were oriented normal to foliations, the B and C cores were cut perpendicular to one another parallel to the foliations, with the axes of the B cores parallel to the strikes of the foliations. The D cores were taken with their axes parallel to the drill core, i.e., vertical (Figure 5). Prior to the velocity measurements, bulk densities were obtained for each minicore from its weight and dimensions.

Velocities were measured using a pulse transmission technique [*Birch*, 1960] to hydrostatic confining pressures of 800 MPa (equivalent to crustal depths of approximately 30 km). The velocities and densities given in Table 2 are estimated to be accurate to 1%.

We have measured velocities to considerably higher pressures than the previous mylonite velocity studies to 100 MPa by *Jones and Nur* [1982]. The reasons for this are twofold. First, the typical velocity versus pressure curve for crystalline rocks generally shows a rapid increase in velocity below 200 MPa which is related to the closing of cracks [*Birch*, 1960]. This is illustrated in Figure 6 for a Brevard phyllonite. Only above 200 MPa are velocities related primarily to mineralogy. Second, it is clear from the textures and mineralogies of the Brevard fault zone mylonites that they originated at intermediate crustal depths corresponding to pressures from 300 MPa to perhaps as high as 600 MPa. Consequently, velocities measured at these pressures will be useful to interpret fault zone reflections from the deeper crust as well as at shallow depths where fault zones have been deeply weathered.

An idealized two-layer model of a major fault zone cutting crystalline quartzofeldspathic crust [*Sibson*, 1977] suggests the probable depth of origin of the Brevard fault zone rocks. At high crustal levels, faulting produces random fabric fault rocks by frictional processes. This overlies a region where quasi-plastic processes of shearing produce mylonites with strong tectonite fabrics similar to the Brevard fault zone rocks which we have studied. As discussed by *Sibson* [1977], the transition depth between these two regions depends on many factors, including temperature and the availability of water, but generally is expected to occur at depths between 10 and 15 km corresponding to pressures of 300–450 MPa.

REFLECTIONS FROM CONTINENTAL CRYSTALLINE FAULT ZONES

Recently, attention has focused on crystalline fault zones as seismic reflectors within the upper continental crust. It has been known for over two decades that if reasonable acoustic impedance contrasts are assumed, the amplitudes

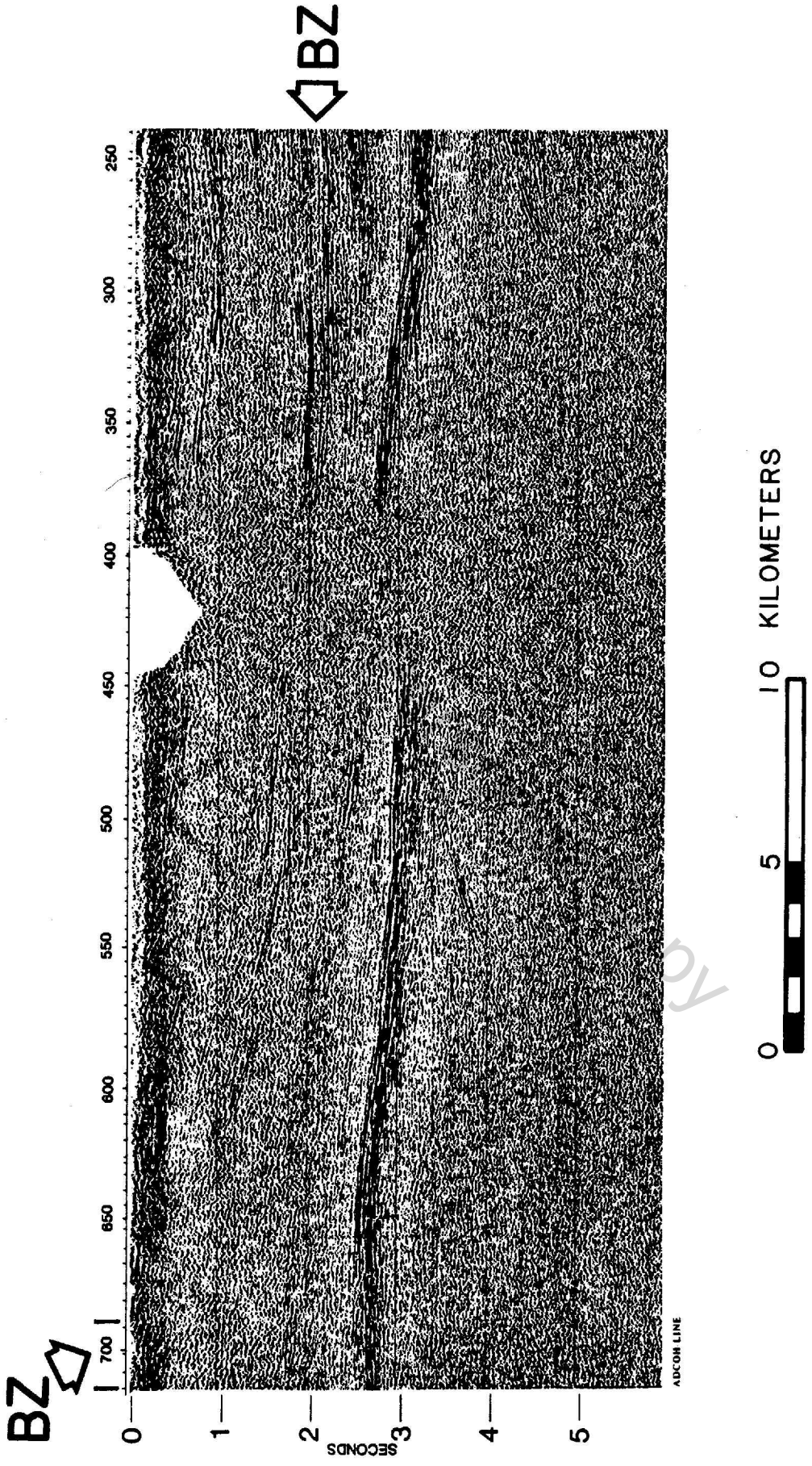

Fig. 2. ADCOH line 1 showing the Brevard fault zone reflectors (BZ). Location of line 1 is shown in Figure 3 (SL-1). The strong reflections at approximately 3.0 s of two-way travel time are interpreted as a lower Paleozoic sedimentary sequence [from *Williams et al.*, 1987].

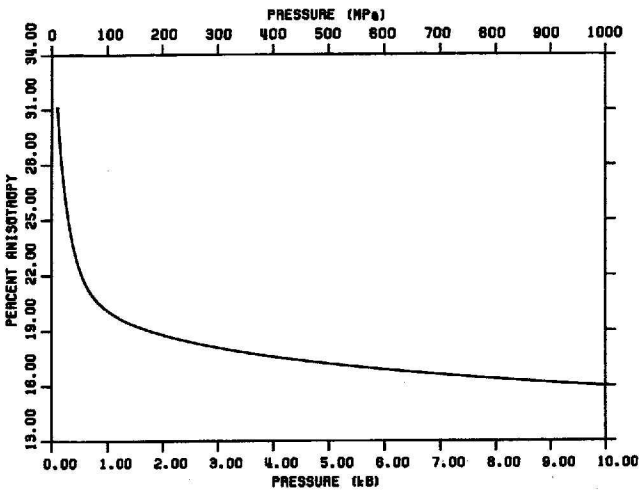

Fig. 7. Percent anisotropy versus pressure for sample at 22.0 m depth. Anisotropy is defined as the difference between the maximum and minimum velocities for a sample expressed as a percentage of the mean velocity.

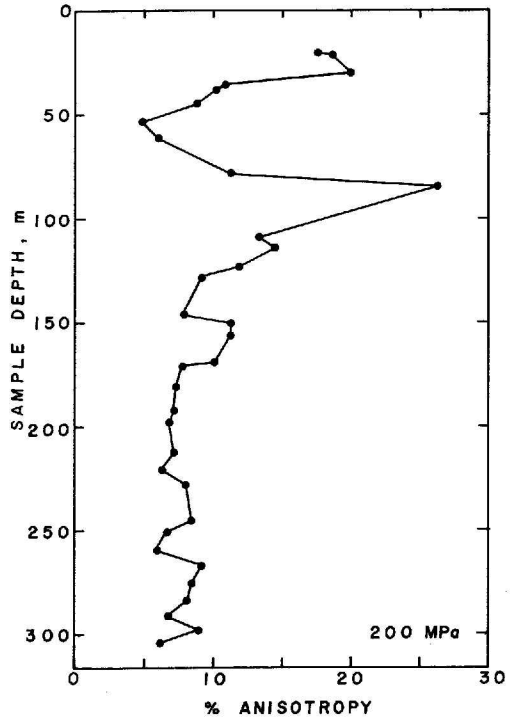

Fig. 9. Percent anisotropy at 200 MPa versus depth.

sponding to a frequency typically exploited in crustal surveys [*Coruh et al.*, 1987]. Although the seismograms consider transmission losses at each interface, no attempt is made to account for dispersion, geometrical spreading, or attenuation. For clarity, the signal-to-noise ratio in these models is infinite. Random noise can generally be expected to deteriorate the coherency, and hence the interpretability, of seismic reflection events. Multiple reflections are not shown.

Each seismogram follows the same format. The vertical axis is total two-way travel time, in seconds. The leftmost trace labeled "D" is a depth scale. Tic marks on this scale appear at 50-m intervals. Since the depth is a function of two-way travel time and velocity, the scale is nonlinear. The velocity model "V" indicates the variation in velocity with sample depth (two-way travel time) between minimum and maximum values. Likewise, "RHO" displays the density data used to calculate the synthetic trace. The "RC" trace shows the reflection coefficient series, with spikes to the right representing positive acoustic impedance contrasts. "SYN" indicates the resulting synthetic seismogram. The trace is shown 7 times to simulate a segment of a zero-offset two-dimensional seismic record. For comparison, a standard trace, "ST," is provided. This trace corresponds to a three-layer model consisting of a +0.1 and a −0.1 reflection coefficient interface. A 0.1 reflection coefficient is comparable to that of a sandstone-limestone contact in a typical sedimentary sequence. By comparing the amplitudes of the model reflections to the standard trace, one can better appreciate the magnitude of the events shown.

Figure 10 illustrates the variation of velocity with direction as a function of sample depth. The length of each horizontal line in the figure is proportional to the anisotropy of the sample. The velocities normal to foliation are always lower than velocities measured parallel to foliation. Figure 10 also demonstrates that samples with greater anisotropy have

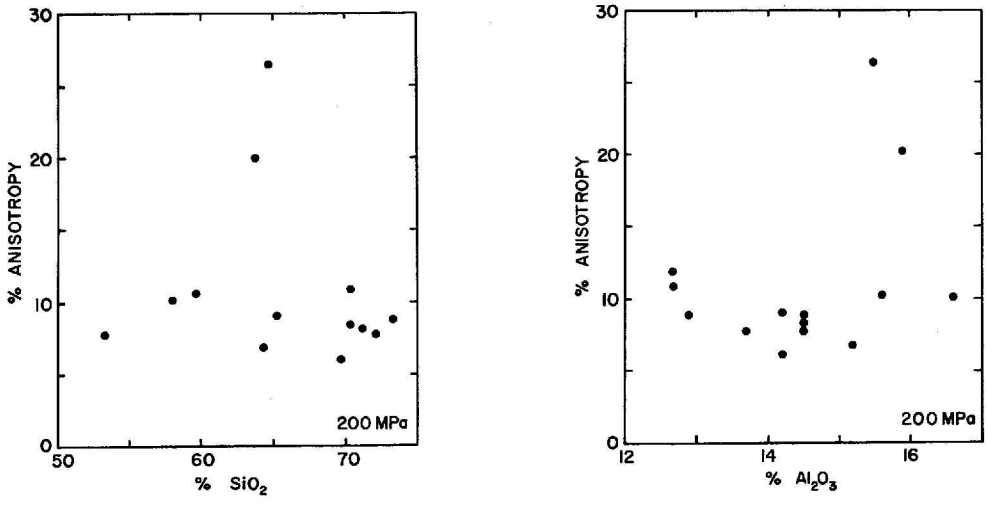

Fig. 8. Percent anisotropy at 200 MPa versus SiO_2 and Al_2O_3 contents.

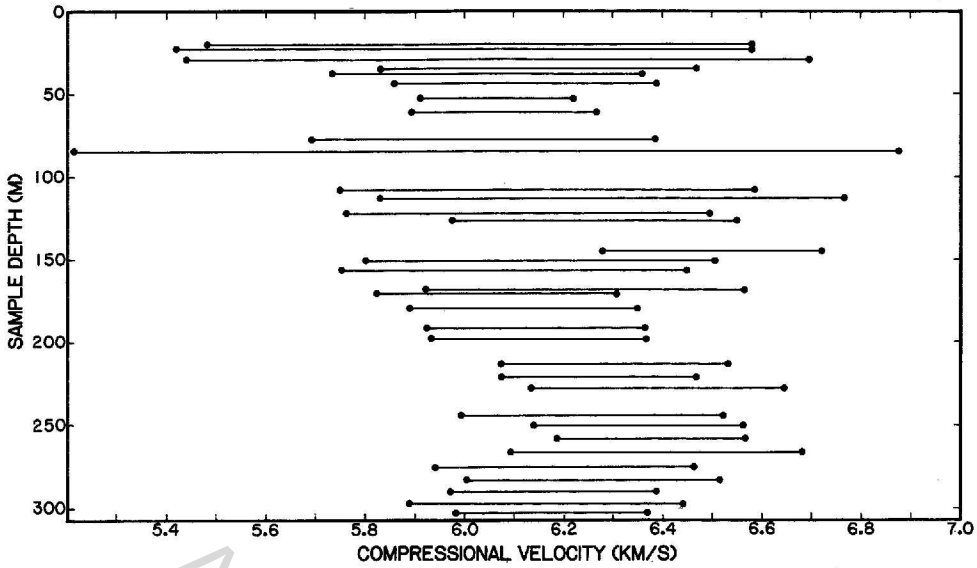

Fig. 10. Minimum and maximum velocities at 200 MPa for three mutually perpendicular cores at each sample depth.

foliation-normal velocities which are consistently lower than samples having lesser anisotropy. This observation suggests a method for considering the effects of anisotropy variations on reflection characteristics largely independent of the effects of chemical variations. If there were neither chemical variations nor anisotropy variations in the core, velocities for all samples would be uniform, approaching the mean velocity of all the samples, which is 6.26 km s^{-1}. However, if anisotropy variations exist, the magnitude of the resulting velocity variation can be expressed as the mathematical product of the percent anisotropy and a velocity constant. This quantity is larger for samples with greater anisotropy and smaller for samples with lesser anisotropy. Because the velocities normal to foliation are consistently lower in the most anisotropic samples, subtracting this product from some constant velocity would create values which are lowest for the samples having the highest anisotropy, which is the velocity behavior observed in Figure 10. To calculate the velocities governed only by anisotropy variations, then, the following equation is used:

$$V_{calc} = 6.26 \text{ km s}^{-1} - (\% \text{ anisotropy})\ (3.84 \text{ km s}^{-1})$$

By this relation, a perfectly isotropic (0% anisotropy) rock would have a calculated velocity of 6.26 km s^{-1}. The sample with highest anisotropy (26.4% at 84.4 m) would have a calculated velocity of 5.25 km s^{-1}; 3.84 km s^{-1} is chosen as the constant velocity value in order to make the average of the calculated velocities equal to the mean velocity of "A" core samples (5.88 km s^{-1}). This method is valid for considering anisotropy variations because of the consistent behavior in the samples of foliation-normal velocities being inversely proportional to percent anisotropy and because using the mean velocity and mean density of all the samples is equivalent to averaging out chemical variations.

Figure 11 shows the synthetic seismogram produced using the calculated velocities. The mean density for all the samples is 2736 kg m^{-3}. The extremely high-amplitude reflection at ~0.025-s two-way travel time results from the significant anisotropy variations observed in the upper 100 m of the hole. In the lower part of the hole, variations in anisotropy are small, and hence reflection amplitudes are negligible. This seismogram indicates that anisotropy variations may be a major contributor to the Brevard fault zone reflectivity.

For the above calculations of the effect of anisotropy on reflections, we used an isotropic modeling technique with a

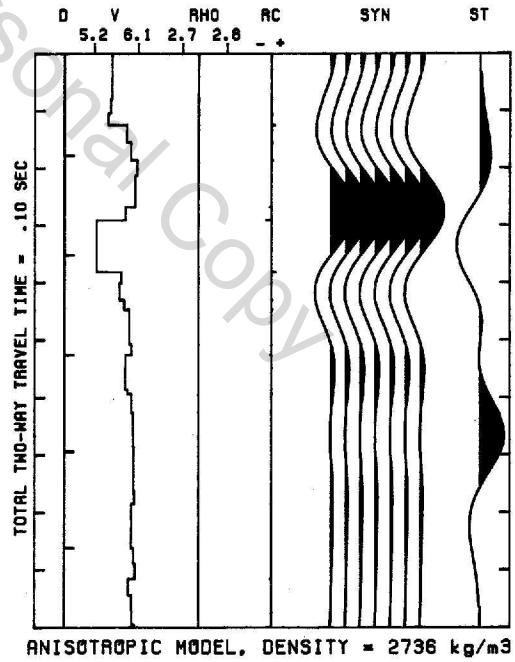

Fig. 11. Reflections originating from anisotropy variations in a hypothetical chemically homogeneous 330-m Brevard fault zone section of uniform density. The vertical axis is total two-way travel time, in seconds. The trace labeled "D" is a depth scale in 50-m intervals. The trace labeled "V" is the velocity model in km s^{-1} and "RHO" is the density model in kg $m^{-3} \times 10^{-3}$. "RC" is the reflection coefficient series, with excursions to the right representing positive acoustic impedance contrasts. "SYN" is the synthetic seismogram, consisting of seven identical traces. A standard trace ("ST"), consisting of a +0.1/−0.1 reflection coefficient interface pair, is provided for amplitude comparison.

TABLE 1. Chemical Analyses

	Brevard Zone Sample Depth, m													Average Shale[a]	Average Granite[b]
	29.0	34.7	43.6	84.4	122.0	126.8	144.8	167.9	170.1	212.5	244.8	274.9	303.9		
SiO_2	63.70	59.70	73.40	64.60	70.40	65.20	53.20	58.00	72.10	64.30	71.20	70.30	69.60	58.10	71.30
TiO_2	1.05	0.61	0.25	1.04	0.85	0.88	1.52	1.10	0.30	0.71	0.38	0.37	0.41	0.60	0.31
Al_2O_3	15.90	12.70	12.90	15.50	12.70	14.20	14.52	16.60	13.70	15.20	14.50	14.50	14.20	15.40	14.30
Fe_2O_3[c]	7.52	6.40	1.69	7.77	5.56	6.30	11.90	8.90	1.94	4.66	2.31	2.57	2.79	4.00	1.21
FeO	...	...	...	...	...	...	...	...	...	...	...	...	...	2.40	1.64
MnO	0.12	0.13	0.07	0.12	0.09	0.10	0.26	0.11	0.07	0.09	0.05	0.06	0.07	...	0.05
MgO	1.99	2.84	0.31	1.70	1.54	1.68	4.22	3.50	0.59	1.84	0.83	0.87	1.01	2.40	0.71
CaO	2.08	6.32	1.11	0.98	1.93	3.13	6.03	3.49	1.71	4.31	1.50	2.29	2.44	3.10	1.84
Na_2O	2.21	2.50	2.91	0.32	2.17	1.89	1.70	2.25	3.80	3.77	4.94	3.96	3.84	1.30	3.68
K_2O	3.69	2.16	5.24	3.62	2.52	2.85	1.51	3.13	3.59	2.51	2.54	3.81	3.57	3.20	4.07
P_2O_5	0.17	0.11	0.06	0.16	0.13	0.18	0.21	0.19	0.09	0.24	0.13	0.13	0.14	0.20	0.12
Cr_2O_3	0.01	0.01	...	0.01	0.01	...	0.01	0.01	...	...	0.01	0.01	0.01	...	...
H_2O[d]	1.62	5.62	1.62	3.77	1.85	2.70	4.77	2.77	2.08	2.16	1.16	0.62	1.08	5.00	0.77
Total	100.20	99.20	99.70	99.70	99.90	99.30	99.90	100.20	100.10	100.00	99.70	99.60	99.30	99.30e	100.07
							Normative								
Q	26.80	19.60	33.10	41.60	39.90	32.10	14.30	17.20	31.20	20.20	27.80	25.80	26.20	34.70	29.10
C	4.90	...	0.57	9.66	3.20	2.75	...	3.62	0.67	...	1.21	0.01	...	9.80	0.92
Or	21.80	12.80	31.00	21.40	14.90	16.80	8.92	18.50	21.20	14.80	15.00	22.50	21.10	18.90	24.10
Ab	18.70	21.20	24.60	2.71	18.40	16.00	14.40	19.00	32.20	31.90	41.80	33.50	32.50	11.00	31.10
An	9.21	17.10	5.11	3.82	8.73	14.40	27.50	16.10	7.90	17.10	6.59	10.50	11.00	...	8.03
Di	...	11.20	...	...	...	...	0.89	...	...	2.20	...	...	0.19	...	...
Hy	11.50	7.62	2.27	11.00	8.54	9.66	20.70	16.60	3.16	7.47	3.99	4.40	4.84	6.09	3.36
Mt	2.56	2.19	0.59	2.64	1.89	2.15	4.08	3.02	0.68	1.59	0.79	0.88	0.96	5.80	1.75
Cm	0.01	0.01	...	0.01	0.01	...	0.01	0.01	...	...	0.01	0.01	0.01	...	...
Il	1.19	1.16	0.47	1.98	1.61	1.67	2.89	2.09	0.57	1.35	0.72	0.70	0.78	1.14	0.59
Ap	0.39	0.25	0.14	0.37	0.30	0.42	0.49	0.44	0.21	0.56	0.30	0.30	0.32	0.46	0.28
Cc	...	...	...	...	...	...	...	...	...	...	...	...	...	5.06	0.11

[a] From *Clarke* [1924].
[b] From *LeMaitre* [1976].
[c] All Fe in Brevard zone samples expressed as Fe_2O_3.
[d] Includes H_2O^+ and H_2O^-.
[e] Remainder of 2.6% CO_2, 0.6% SO_3, 0.8% C.

reflection to weaken or die out. Considering again the possibility of anomalously high pore pressures, they concluded that the permeabilities required to maintain high pore pressure are unrealistically small.

REFLECTIONS FROM THE BREVARD FAULT ZONE

Field and laboratory investigations of fault zones suggest a layered source geometry for fault zone reflections. Two proposed origins for the laminations merit further consideration here. First, heterogeneity in composition may exist within fault zones such that layers of sufficiently large impedance contrasts and appropriate thicknesses produce the reflections. This is reasonable since major fault zones are likely to cut a wide variety of lithologies which become intimately interlayered subparallel to the fault zone due to movement along the fault zone. Second, variations of seismic anisotropy within the fault zone may produce the observed reflections. In the ductile regime of fault zones, preferred mineral orientation will produce a variation of velocity with direction in mylonites. In the Brevard fault zone rocks, mica is the major contributor to this anisotropy. The laminations producing the reflections could simply be regions within the fault zone with differing magnitudes of anisotropy, originating from variations in the abundance and degree of preferred orientation of mica. For shallow-dipping fault zones with mylonite foliation nearly horizontal, velocities measured perpendicular to foliation would be critical in investigating a possible anisotropic origin for near-vertical reflections.

Seismic anisotropy is a significant physical property of the Brevard fault zone mylonites. Anisotropies expressed as percents are given in Table 3 as functions of depth and confining pressure. Following *Birch* [1960], anisotropy is defined as the difference between the maximum and minimum velocities in a sample expressed as a percentage of the

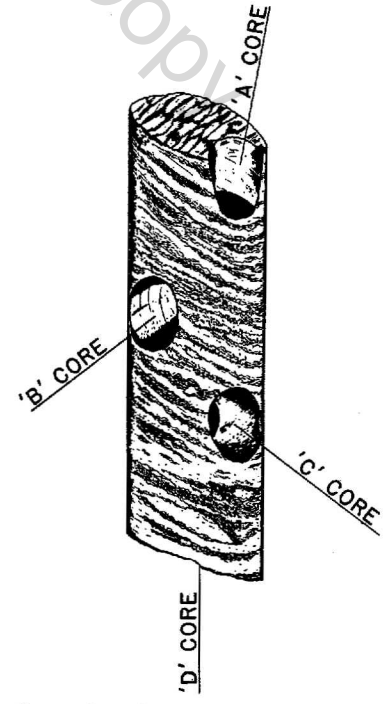

Fig. 5. Core orientations for anisotropy measurements.

TABLE 2. Compressional Wave Velocity as a Function of Pressure

Sample Depth, m	Orientation	Density, kg m^{-3}	P, MPa 20	40	60	80	100	200	400	600	800
20.3	A	2791	4.87	5.08	5.20	5.28	5.33	5.46	5.56	5.61	5.65
	B	2785	6.29	6.38	6.44	6.48	6.50	6.56	6.61	6.64	6.65
	D	2811	4.78	5.00	5.12	5.20	5.24	5.37	5.48	5.55	5.60
22.0	A	2784	4.73	5.01	5.15	5.23	5.28	5.40	5.52	5.59	5.64
	B	2785	6.32	6.40	6.44	6.48	6.50	6.56	6.62	6.65	6.68
	D	2781	4.76	5.02	5.17	5.26	5.33	5.48	5.58	5.64	5.68
29.0	A	2788	4.69	4.94	5.09	5.19	5.27	5.44	5.55	5.62	5.66
	B	2792	6.32	6.45	6.52	6.56	6.60	6.68	6.76	6.81	6.84
	C	2766	6.16	6.26	6.33	6.38	6.41	6.51	6.60	6.65	6.68
	D	2788	5.00	5.19	5.30	5.37	5.42	5.58	5.72	5.81	5.88
34.7	A	2783	5.25	5.46	5.58	5.65	5.70	5.82	5.93	5.99	6.03
	B	2783	6.06	6.17	6.25	6.30	6.34	6.46	6.53	6.56	6.58
	C	2769	6.07	6.15	6.20	6.23	6.25	6.34	6.42	6.47	6.51
	D	2770	5.57	5.64	5.68	5.72	5.74	5.84	5.91	5.94	5.96
37.3	A	2760	5.07	5.30	5.45	5.56	5.63	5.80	5.91	5.96	6.00
	B	2745	6.07	6.18	6.25	6.30	6.34	6.44	6.52	6.56	6.59
	C	2757	5.92	6.04	6.12	6.18	6.23	6.34	6.42	6.45	6.48
	D	2760	5.08	5.27	5.39	5.47	5.53	5.69	5.81	5.87	5.92
43.6	A	2656	4.75	5.09	5.32	5.49	5.61	5.88	6.00	6.06	6.10
	B	2654	5.80	5.94	6.03	6.09	6.14	6.26	6.33	6.36	6.38
	C	2629	5.66	5.85	5.99	6.09	6.17	6.37	6.49	6.53	6.56
	D	2652	4.72	5.03	5.24	5.38	5.48	5.72	5.85	5.24	5.96
52.8	A	2656	5.00	5.31	5.51	5.64	5.73	5.92	6.02	6.07	6.10
	B	2650	5.70	5.85	5.95	6.03	6.08	6.22	6.30	6.34	6.36
	C	2655	5.56	5.74	5.86	5.95	6.02	6.18	6.26	6.29	6.32
	D	2657	5.03	5.39	5.60	5.72	5.79	5.96	6.08	6.16	6.21
60.9	A	2684	5.55	5.65	5.72	5.76	5.80	5.91	5.99	6.04	6.07
	B	5685	5.87	6.00	6.08	6.13	6.17	6.27	6.33	6.37	6.40
	D	2686	5.21	5.43	5.58	5.68	5.75	5.91	6.01	6.07	6.11
77.6	A	2752	5.20	5.31	5.39	5.45	5.51	5.68	5.81	5.86	5.88
	B	2755	6.17	6.23	6.26	6.28	6.30	6.36	6.41	6.45	6.47
	C	2797	6.18	6.25	6.28	6.31	6.33	6.39	6.46	6.50	6.54
	D	2750	5.50	5.57	5.63	5.67	5.71	5.83	5.93	5.96	5.98
84.4	A	2819	3.92	4.35	4.62	4.80	4.92	5.21	5.43	5.56	5.66
	B	2800	6.52	6.62	6.69	6.74	6.78	6.88	6.94	6.96	6.98
	D	2789	5.05	5.17	5.25	5.31	5.36	5.54	5.74	5.86	5.94
108.0	A	2808	5.33	5.47	5.55	5.61	5.65	5.76	5.84	5.89	5.93
	B	2796	6.42	6.47	6.50	6.52	6.54	6.58	6.63	6.66	6.68
	C	2817	6.30	6.38	6.43	6.46	6.48	6.54	6.60	6.63	6.66
	D	2789	5.41	5.55	5.65	5.71	5.76	5.88	5.96	6.01	6.04
113.6	A	2842	5.64	5.70	5.74	5.76	5.78	5.85	5.91	5.95	5.97
	B	2853	6.62	6.66	6.68	6.70	6.71	6.75	6.80	6.82	6.84
	C	2870	6.40	6.46	6.49	6.52	6.54	6.59	6.65	6.69	6.71
	D	2844	5.63	5.70	5.74	5.76	5.79	5.85	5.92	5.96	5.99
122.0	A	2748	5.39	5.51	5.57	5.62	5.65	5.75	5.84	5.90	5.94
	B	2745	6.27	6.34	6.38	6.40	6.43	6.48	6.54	6.57	6.59
	C	2739	6.14	6.21	6.25	6.28	6.30	6.37	6.45	6.49	6.52
	D	2752	5.49	5.59	5.65	5.69	5.72	5.82	5.91	5.97	6.02
126.8	A	2749	5.65	5.76	5.82	5.87	5.90	5.97	6.04	6.08	6.11
	B	2751	6.29	6.36	6.40	6.43	6.45	6.52	6.60	6.64	6.67
	C	2747	6.07	6.16	6.21	6.25	6.27	6.34	6.40	6.43	6.46
	D	2750	5.65	5.77	5.83	5.88	5.91	5.98	6.05	6.09	6.12
144.8	A	2837	6.02	6.08	6.11	6.14	6.15	6.21	6.28	6.31	6.34
	B	2751	6.40	6.43	6.45	6.46	6.47	6.51	6.55	6.57	6.58
	C	2765	6.49	6.56	6.60	6.63	6.65	6.71	6.78	6.83	6.86
	D	2765	6.06	6.12	6.16	6.18	6.20	6.25	6.31	6.35	6.38
150.2	A	2731	5.38	5.52	5.60	5.66	5.70	5.81	5.88	5.92	5.95
	B	2727	6.33	6.38	6.40	6.42	6.44	6.49	6.55	6.59	6.62
	D	2780	5.29	5.41	5.48	5.53	5.57	5.66	5.73	5.77	5.80
156.3	A	2718	5.54	5.59	5.63	5.65	5.68	5.75	5.83	5.87	5.89
	B	2721	6.23	6.30	6.34	6.36	6.38	6.45	6.52	6.56	6.58
	C	2743	6.24	6.27	6.29	6.31	6.32	6.37	6.44	6.48	6.51
	D	2733	5.58	5.63	5.66	5.69	5.71	5.77	5.84	5.88	5.91
167.9	A	2801	5.73	5.79	5.82	5.85	5.87	5.93	6.01	6.06	6.10
	B	2772	6.33	6.37	6.39	6.41	6.43	6.47	6.52	6.54	6.56
	C	2828	6.41	6.46	6.48	6.50	6.51	6.56	6.62	6.66	6.68
	D	2805	5.82	5.92	5.99	6.03	6.06	6.14	6.22	6.27	6.30
170.1	A	2659	4.99	5.27	5.45	5.58	5.66	5.83	5.92	5.96	6.00
	B	2668	5.98	6.07	6.13	6.18	6.21	6.32	6.37	6.39	6.40
	D	2674	5.31	5.46	5.57	5.65	5.71	5.89	6.01	6.05	6.08

TABLE 2. (continued)

Sample Depth, m	Orientation	Density, kg m^{-3}	P, MPa 20	40	60	80	100	200	400	600	800
179.8	A	2697	4.77	5.18	5.43	5.60	5.70	5.91	6.00	6.05	6.09
	B	2695	5.70	5.91	6.05	6.14	6.20	6.33	6.39	6.42	6.44
	C	2698	5.90	6.09	6.18	6.22	6.26	6.35	6.44	6.49	6.53
	D	2716	4.78	5.18	5.44	5.61	5.73	5.96	6.06	6.11	6.14
191.2	A	2691	4.73	5.18	5.46	5.63	5.74	5.94	6.03	6.08	6.11
	B	2700	5.76	6.01	6.15	6.23	6.28	6.37	6.43	6.46	6.48
	C	2705	5.75	6.00	6.13	6.20	6.24	6.31	6.36	6.39	6.41
	D	2702	5.06	5.48	5.68	5.79	5.86	5.96	6.03	6.07	6.11
197.6	A	2691	4.71	5.21	5.50	5.68	5.78	5.96	6.04	6.09	6.12
	B	2689	5.90	6.07	6.18	6.24	6.29	6.37	6.42	6.45	6.46
	C	2688	5.64	5.90	6.05	6.13	6.19	6.30	6.37	6.42	6.45
	D	2673	4.93	5.22	5.41	5.53	5.62	5.81	5.93	6.00	6.04
212.5	A	2719	5.53	5.77	5.90	5.96	6.00	6.09	6.16	6.20	6.23
	B	2725	6.12	6.26	6.35	6.40	6.43	6.50	6.56	6.58	6.61
	C	2738	5.93	6.16	6.29	6.37	6.42	6.53	6.59	6.63	6.66
	D	2741	5.20	5.63	5.85	5.98	6.05	6.19	6.29	6.35	6.39
220.5	A	2702	5.25	5.61	5.80	5.91	5.97	6.08	6.15	6.19	6.22
	B	2709	6.12	6.24	6.31	6.36	6.39	6.47	6.52	6.56	6.58
	C	2699	5.83	6.05	6.17	6.24	6.28	6.37	6.45	6.49	6.53
	D	2707	5.14	5.50	5.70	5.81	5.88	6.01	6.08	6.13	6.16
227.3	A	2774	5.40	5.72	5.88	5.98	6.04	6.14	6.20	6.24	6.27
	B	2759	6.25	6.39	6.47	6.52	6.56	6.63	6.68	6.71	6.74
	C	2746	5.93	6.13	6.24	6.31	6.35	6.43	6.50	6.54	6.56
	D	2759	5.41	5.72	5.89	5.99	6.04	6.14	6.20	6.24	6.26
244.8	A	2654	5.23	5.64	5.81	5.89	5.93	6.01	6.08	6.12	6.15
	B	2666	5.87	6.07	6.17	6.21	6.24	6.32	6.38	6.42	6.45
	C	2657	5.99	6.23	6.34	6.40	6.43	6.51	6.57	6.60	6.63
	D	2678	5.70	5.84	5.91	5.96	5.98	6.06	6.14	6.19	6.22
250.4	A	2760	5.73	5.86	5.94	6.00	6.04	6.13	6.20	6.24	6.27
	B	2771	6.26	6.36	6.42	6.46	6.49	6.57	6.62	6.65	6.67
	C	2760	6.14	6.29	6.37	6.41	6.44	6.51	6.57	6.61	6.63
	D	2770	5.72	5.87	5.96	6.01	6.05	6.13	6.21	6.25	6.29
258.5	A	2753	5.55	5.78	5.92	6.00	6.06	6.19	6.30	6.36	6.41
	B	2750	6.05	6.23	6.35	6.42	6.47	6.57	6.63	6.65	6.67
	D	2718	5.45	5.70	5.85	5.94	6.00	6.13	6.20	6.24	6.27
266.5	A	2773	5.39	5.66	5.81	5.90	5.96	6.08	6.16	6.22	6.25
	B	2769	6.22	6.36	6.46	6.53	6.57	6.69	6.75	6.77	6.79
	C	2768	5.93	6.13	6.24	6.31	6.35	6.44	6.51	6.55	6.58
	D	2760	5.31	5.60	5.76	5.86	5.92	6.05	6.14	6.18	6.22
274.9	A	2688	4.81	5.32	5.58	5.73	5.82	5.97	6.07	6.13	6.17
	B	2699	5.87	6.10	6.24	6.32	6.37	6.47	6.53	6.57	6.59
	C	2712	5.63	5.91	6.09	6.19	6.27	6.42	6.52	6.57	6.61
	D	2729	5.14	5.47	5.66	5.77	5.83	5.96	6.04	6.09	6.12
282.8	A	2711	5.31	5.62	5.78	5.87	5.93	6.03	6.09	6.13	6.16
	B	2722	6.16	6.28	6.35	6.40	6.43	6.51	6.56	6.59	6.61
	C	2707	5.92	6.07	6.16	6.22	6.25	6.33	6.38	6.41	6.43
	D	2709	5.05	5.50	5.71	5.82	5.88	5.98	6.05	6.09	6.11
290.2	A	2697	5.16	5.48	5.67	5.78	5.85	5.98	6.06	6.10	6.13
	B	2663	6.15	6.23	6.28	6.31	6.33	6.37	6.41	6.43	6.45
	D	2687	5.28	5.62	5.80	5.91	5.97	6.09	6.18	6.23	6.27
297.5	A	2688	5.01	5.32	5.51	5.64	5.72	5.90	6.00	6.06	6.10
	B	2704	5.89	6.13	6.25	6.32	6.37	6.45	6.50	6.54	6.56
	D	2700	5.05	5.40	5.60	5.73	5.81	5.96	6.04	6.09	6.13
303.9	A	2692	4.66	5.25	5.56	5.73	5.83	5.99	6.09	6.15	6.19
	B	2683	5.66	5.92	6.07	6.16	6.22	6.34	6.41	6.45	6.48
	C	2682	5.49	5.87	6.09	6.20	6.27	6.37	6.43	6.47	6.49
	D	2673	4.94	5.41	5.65	5.78	5.86	6.00	6.10	6.16	6.20

Velocities are in kilometers per second.

mean. In general, the behavior of anisotropy with pressure is affected in a manner similar to velocity (Figure 7). At low pressures, anisotropies of the mylonites are enhanced by oriented microcracks. At pressures above 200 MPa the anisotropies are primarily related to the preferred orientation of phyllosilicates (Figure 4) and are similar to those of regionally metamorphosed quartzofeldspathic schists in which the abundance and degree of orientation of mica control their magnitudes [*Christensen*, 1965]. Compressional wave velocities are slow for propagation directions normal or nearly normal to the foliation and fast for propagation in the foliation. For a few samples the slowest velocities were measured in the vertical direction rather than normal to the foliation. Petrographic examination of these samples showed shingled or sometimes crenulated micas (*c*-surfaces) with concentrations of (001) normals (the slowest direction in mica) several degrees away from foliation normals.

The degree of anisotropy in the Brevard fault zone

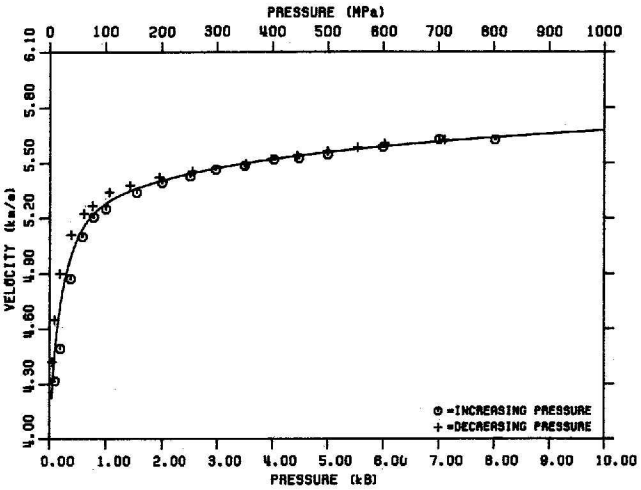

Fig. 6. Compressional wave velocity as a function of pressure for the A core at 22.0 m depth.

mylonites does not appear to be related in a simple manner to chemistry. Anisotropy percentages and SiO_2 contents show no correlation (Figure 8). Two of the more highly anisotropic samples (29.0 and 84.4 m) contain high Al_2O_3, which is expected in samples with abundant mica. However, the other samples seem to show an unexpected decrease in anisotropy with increasing Al_2O_3 content.

Anisotropy varies considerably with depth within the cored section of the fault zone (Figure 9). In the upper 150 m, anisotropies at 200 MPa decrease from 20 to 5%, then increase to over 26% and decrease again to less than 7%. Within the lower 100 m of the corehole, anisotropy at 200 MPa fluctuates between 5 and 10%.

In the remainder of the paper we make extensive use of synthetic seismograms to examine how various factors govern the reflection character of the Brevard fault zone. Figures 11, 13, and 14 consider the reflection patterns resulting from anisotropy variations, chemical variations, and a combination of the two factors, respectively. Figure 15 presents a simplistic treatment of the effects of dipping foliation. As a final case, we use a random vertical distribution of Brevard fault zone lithologies to demonstrate the inherent reflectivity of these units (Figure 16). A thorough discussion of the results of the seismic modeling follows.

The seismograms attempt to emulate the behavior of a seismic wave impinging with normal incidence upon a plane layer geology [*Wuenschel*, 1960; *Robinson and Treitel*, 1977]. Velocity data at 200 MPa are used in the models. This pressure corresponds to crustal conditions at 6–7 km depth and is above the microcrack closure region in the samples. With the laboratory density and velocity information and an estimation of thicknesses of lithologic units in the core, a reflection coefficient time series is constructed. This series is convolved with a zero phase, three extrema wavelet to produce the seismograms. A 25-Hz wavelet is used, corre-

TABLE 3. Compressional Wave Anisotropy as a Function of Pressure

Sample Depth, m	*P*, MPa 20	40	60	80	100	200	400	600	800
20.3	24.3	21.9	20.6	19.8	19.2	17.9	16.9	16.3	15.9
22.0	27.3	23.4	21.6	20.6	20.1	18.8	17.6	16.9	16.4
29.0	28.5	25.7	23.8	22.6	21.8	20.1	19.2	18.8	18.5
34.7	14.1	12.1	11.2	10.7	10.5	10.2	9.6	9.1	8.7
37.3	17.6	15.1	13.5	12.4	11.7	10.3	9.7	9.4	9.3
43.6	19.5	15.0	12.2	10.2	9.4	8.1	7.7	7.4	7.2
52.8	12.9	9.6	7.7	6.5	5.8	4.8	4.5	4.3	4.2
60.9	5.5	5.9	6.1	6.1	6.1	5.8	5.5	5.3	5.2
77.6	16.7	15.6	14.6	13.8	13.2	11.1	9.7	9.4	9.4
84.4	46.0	38.7	34.6	32.0	30.2	26.4	23.4	21.5	20.1
108.0	18.2	16.4	15.4	14.7	14.2	13.2	12.4	11.9	11.6
113.6	15.7	15.2	15.0	14.8	14.6	14.2	13.7	13.4	13.2
122.0	14.8	13.8	13.2	12.9	12.6	11.8	11.0	10.6	10.3
126.8	10.5	9.8	9.4	9.1	9.0	8.8	8.8	8.8	8.8
144.8	7.4	7.5	7.6	7.6	7.7	7.7	7.8	7.8	7.8
150.2	15.8	14.2	13.1	12.3	11.8	10.8	10.6	10.5	10.6
156.3	11.6	11.7	11.7	11.6	11.6	11.3	11.0	10.9	11.0
167.9	11.1	10.8	10.5	10.4	10.3	9.9	9.5	9.3	9.1
170.1	17.6	13.7	11.4	10.0	9.2	7.8	7.3	6.8	6.5
179.8	20.8	15.9	12.6	10.5	9.1	7.1	6.9	6.0	6.9
191.2	19.0	14.4	11.7	10.0	8.8	6.9	6.3	6.1	5.9
197.6	21.9	15.0	11.4	9.4	8.3	6.6	6.0	5.7	5.4
212.5	10.0	8.0	7.3	7.0	6.8	6.9	6.8	6.7	6.6
220.5	15.3	10.7	8.5	7.4	6.8	6.1	5.8	5.7	5.6
227.3	14.5	11.1	9.5	8.7	8.2	7.7	7.4	7.3	7.2
244.8	13.4	9.8	8.7	8.4	8.2	8.0	7.7	7.6	7.5
250.4	8.7	8.0	7.6	7.4	7.2	6.8	6.5	6.3	6.2
258.5	8.5	7.4	7.0	6.7	6.5	5.9	5.0	4.4	4.0
266.5	14.2	11.6	10.5	10.0	9.8	9.5	9.0	8.6	8.2
274.9	19.4	13.6	11.0	9.6	8.9	7.9	7.3	7.0	6.9
282.8	14.6	11.0	9.4	8.6	8.1	7.6	7.4	7.3	7.2
290.2	16.9	12.5	10.0	8.6	7.7	6.2	5.6	5.2	5.0
297.5	15.8	13.7	12.3	11.2	10.5	8.8	8.0	7.5	7.2
303.9	18.9	11.7	9.0	7.8	7.2	6.1	5.4	5.1	4.8

Anisotropy is given in percentage.

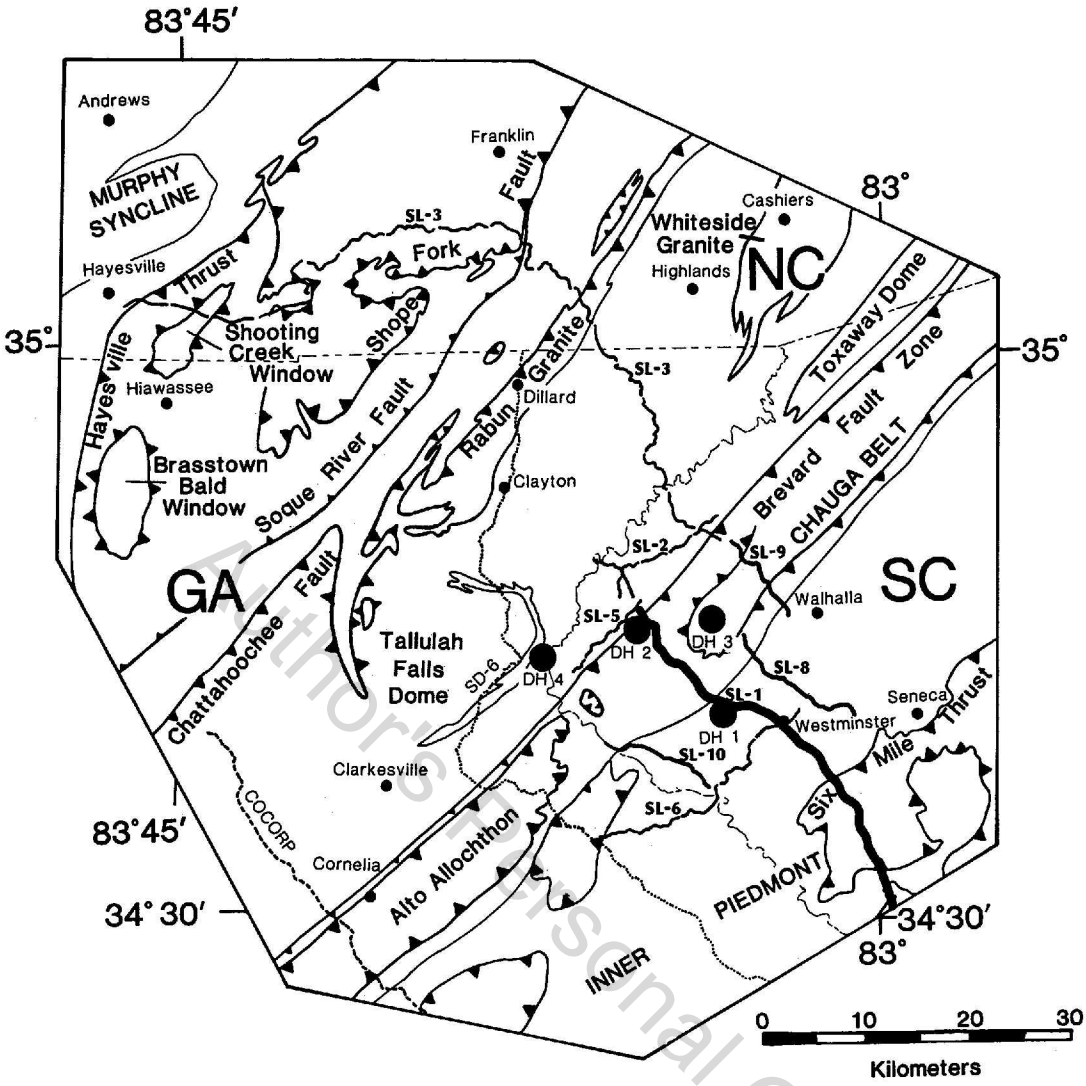

Fig. 3. Map showing locations of core holes (DH1–DH4), seismic reflection lines, and major structural features in the vicinity of the proposed ultradeep core hole. Heavy line indicates location of seismic line (SL-1) of Figure 2 [from *Hatcher et al.*, 1987].

of crustal reflections are larger than expected from first-order discontinuities [*O'Brien*, 1965]. In particular, the strong reflections commonly associated with major crustal fault zones are unlikely to originate from a planar contact separating fault zone rock from its protolith. *Fuchs* [1969], in a classic paper dealing with deep crustal reflections in central Europe, observed that laminated zones with velocity reversals produce high-amplitude reflections consistent with field records. For a minimum-phase wavelet the reflectivity of laminated media reaches a high value if the layer thicknesses are a quarter wavelength. Thus some type of layering is necessary to produce the strong reflections characteristic of fault zones.

The Wind River thrust in Wyoming, which places Precambrian migmatites on nearly flat-lying Paleozoic through early Tertiary sedimentary strata, appears on COCORP records as a zone of strong, relatively continuous reflectors approximately 0.5 s of two-way travel time (~1.5 km) in thickness. The fault zone dips 30°–40° northeast and is traceable to a depth of about 20 km; it may cut through the crust to the mantle. The thickness of the reflector package associated with the fault zone appears to increase with depth. *Smithson et al.* [1979] suggested that these high-amplitude reflections result from the juxtaposition of contrasting lithologies across the fault, the presence of a mylonite zone along the fault, or a combination of the two effects.

Similarly, the British Institutions Reflection Profiling Syndicate (BIRPS) surveys have imaged continental crystalline fault zones penetrating both the crust and mantle. The package of reflectors associated with each zone is 0.3–0.5 s thick (two-way travel time), or greater. *Matthews and Cheadle* [1986] remarked that although the origin of reflections from fault zones is poorly understood, mylonites may provide sufficient acoustic impedance contrasts. They suggested, however, that localization of volatiles within the fault zone is responsible for the reflections.

Mylonite zones are also associated with metamorphic core complexes in the western Cordillera. Core complexes have been interpreted as products of extreme extension. The brittlely deformed cover rocks are separated from the underlying ductilely deformed core by a low-angle detachment

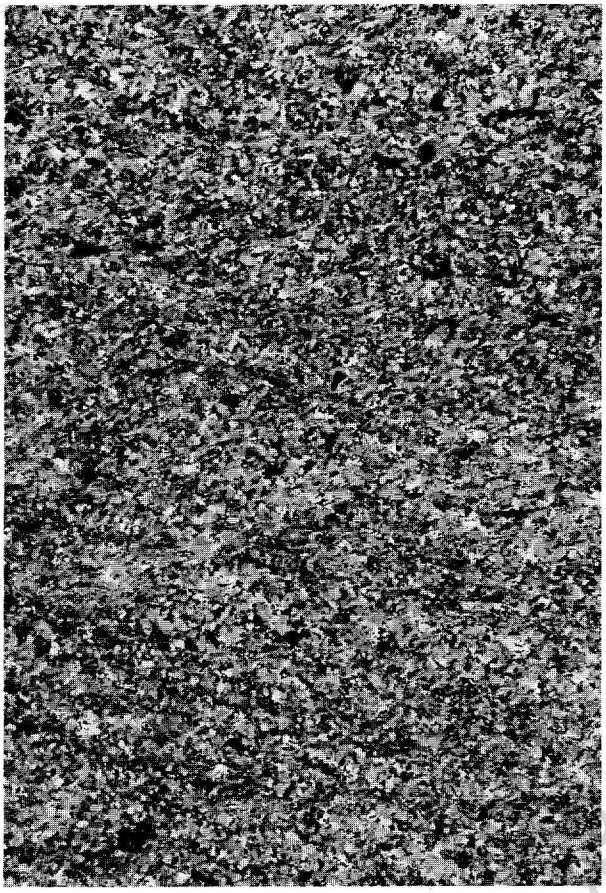

Fig. 4. Photomicrograph of phyllonite from 20.3 m depth showing recrystallization textures and the preferred mica orientation. Width of photo equals 1 cm.

fault, or decollement. Mechanical behavior of materials in the detachment zone varies from brittle (breccia) to ductile (mylonite) [*Davis*, 1980; *Armstrong*, 1982]. Seismic data over the Picacho Mountains in Arizona indicated layered reflectors at a depth of about 1.7 s two-way travel time. These were interpreted as sedimentary layers which had been overthrust by Precambrian granite. However, a wildcat well was drilled through several of the reflecting horizons, revealing compositionally layered and ductilely deformed granodioritic gneiss [*Reif and Robinson*, 1981].

McCarthy [1986] examined seismic data over the northern Snake Range metamorphic core complex in Nevada. McCarthy suggested that anastomosing shear zones, layered intrusives, stretching fabrics and transposed compositional layering produced during extension would contribute to the reflectivity observed on seismic records.

Hurich et al. [1986] conducted a seismic reflection survey of the Kettle Dome metamorphic core complex in Washington state. Reflection events were observed, and once again it was speculated that these reflections resulted from mylonitically layered rock of appropriate geometry for constructive interference.

Published laboratory studies of the seismic properties of mylonitic rocks are limited to a few measurements obtained to a maximum confining pressure of 100 MPa. *Clark et al.* [1978] used ultrasonic velocity measurements of surface samples from the Brevard fault zone to construct their cross section. They reported only one velocity: 5.6 km s^{-1} for the Henderson Gneiss, with no mention made of confining pressure. Velocity analyses of their seismic data yielded a 5.9 km s^{-1} velocity for the section interpreted as the Brevard fault zone. *Jones and Nur* [1982] made the first thorough velocity measurements on a suite of crystalline fault rocks consisting of five undeformed granodiorite protolith specimens, two mylonitic granodiorites, five mylonitic metasedimentary rocks, one flaser gneiss mylonite, one blastomylonitic quartzite, and one cataclasite. Greatest velocity anisotropy was observed in their micaceous quartzite (21%). Anisotropy in the mylonitic granodiorites measured 2% and 5%. Jones and Nur attributed the high anisotropies of the metasedimentary rocks to an aphanitic texture, a high content of phyllosilicates, and a pervasive foliation. Since only a slight acoustic impedance contrast existed between their granodioritic protolith and mylonite, they concluded that the fault zone reflections could not be produced by the juxtaposition of isotropic protolith and anisotropic mylonite. In addition, Jones and Nur noted that most protoliths are low in mica, which is primarily responsible for anisotropy. They assumed that mylonites have mineralogies similar to their protoliths and thus have low anisotropies. They suggested instead a compositional banding of mafic and felsic minerals within the fault zone or anomalously high pore pressures as causes of the observed reflections.

Etheridge and Vernon [1983] pointed out that protolith and mylonite mineral assemblages often are quite different because of reactions such as the replacement of potash feldspar by muscovite and quartz during mylonitization. Thus they contended that the conclusion of *Jones and Nur* [1982] that mylonitic rocks are expected to have generally low-velocity anisotropy was unjustified.

Fountain et al. [1984] considered the reflectivity of mylonite zones through the use of synthetic seismograms. They used a small reflection coefficient of 0.03 based on the velocity and density data of *Jones and Nur* [1982] and concluded that laminated mylonite zones with low reflection coefficients can produce reflections similar to those on seismic records. Amplitudes may be twice those of a simple interface, due to interference effects. By modeling the anastomosing geometry of a mapped surface mylonite zone and rotating the model into a vertical plane to simulate a vertical cross-section, they showed that events are correlatable across the profile but amplitudes vary laterally. The reflectivity of mylonite zones is due, in their estimation, to layers rich in oriented phyllosilicates alternating with unmylonitized, seismically isotropic layers. They suggested that zones of anomalously high pore pressure need not be present to account for the reflections.

In 1984, *Jones and Nur* [1984] added two mylonite samples and four protolith gneisses to their 1982 suite of 100-MPa velocity measurements. These samples came from the Bartletts Ferry and Goat Rock fault zones in Alabama. Jones and Nur also analyzed the frequency spectra of the Wind River data and determined the source of the fault zone reflections to be a laminar structure of alternating high- and low-velocity layers, each 100–150 m thick. These thicknesses are appropriate for constructive interference of the seismic source wavelet, which could have produced large-amplitude events from relatively small acoustic impedance contrasts. Modeling of the Wind River data using the velocities measured on the mylonites in the lab indicated strong reflections for a laminated geometry with anisotropy of 7% or greater. They added that this result is very thickness dependent and lateral changes in thickness could cause a

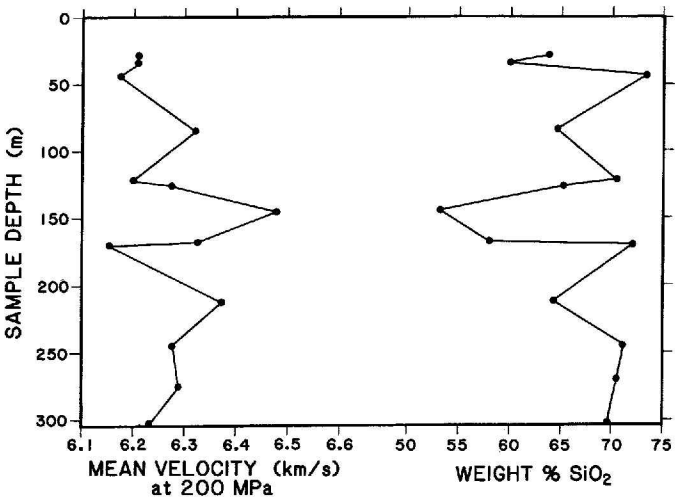

Fig. 12. Mean velocity at 200 MPa and percent SiO_2 versus depth.

velocity function representing the fractional velocity perturbation due to anisotropy in the direction of normal incidence. We believe this approach is valid for Brevard fault zone rocks with nearly horizontal foliations. Greenschist and amphibolite facies micaceous rocks similar to the Brevard rocks, to a first approximation, are often transversely isotropic with their symmetry axes normal to foliation [*Christensen*, 1965, 1966]. For seismic waves traveling parallel to the axis the rock behaves as an isotropic solid (i.e., only two distinct modes of propagation exist having particle motion parallel and perpendicular to the symmetry axis). For this propagation direction the compressional and shear waves are pure modes, and shear wave splitting does not occur. For near-vertical reflection profiling in fault zone rocks with horizontal foliations, wave propagation approximately parallels this symmetry axis. If the foliation is vertical or steeply dipping, the use of an anisotropic method for calculating the synthetic seismograms may be necessary.

Chemical variations also influence velocity and density behavior and hence reflection characteristics. Figure 12 shows the mean compressional velocities of samples for which chemical analyses were obtained. Mean compressional velocity for each sample varies inversely with weight percent SiO_2. Although this relationship is generally expected, we were surprised by the amount of SiO_2 variation, which was not particularly visible in the core. A synthetic seismogram (Figure 13) considers the effects of this chemical variation independent of the effects of anisotropy fluctuations. Anisotropy effects were negated by averaging the three mutually perpendicular velocities for each sample interval, which is equivalent to measuring the velocity in an isotropic sample of identical composition [*Christensen and Ramananantoandro*, 1971]. Densities were also averaged at each sample depth. In Figure 13 the velocity and density jump at ~0.025-s two-way travel time, corresponding to a graphitic phyllonite unit at 84 m depth, produces a broad reflection trough. Chemical variation in the lower two thirds of the hole gives rise to lower-amplitude reflections. Although not as dramatic as the anisotropy-related reflection, this seismogram supports the idea that fault zones in crystalline terranes are reflective due in part to the chemical variability of the fault zone lithologies.

In reality, a near-vertical incidence reflection survey would encounter the effects of both chemical and anisotropy

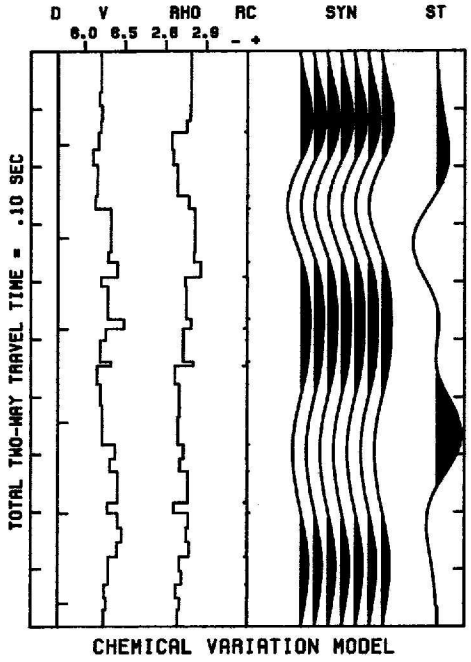

Fig. 13. Reflections originating from chemical variations in a hypothetical isotropic 330-m Brevard fault zone section. For details of plot structure refer to Figure 11 caption and text.

variations. Such a record could be simulated using the velocities and densities measured in the cores oriented normal to foliation (the A cores). The seismic model (Figure 14) reveals that the vertical incidence seismogram is the result of superpositioning of anisotropy and chemical variation effects. This is particularly evident in the upper part of the hole, where the high-amplitude reflection due to anisotropy variation has been reduced by offsetting chemical

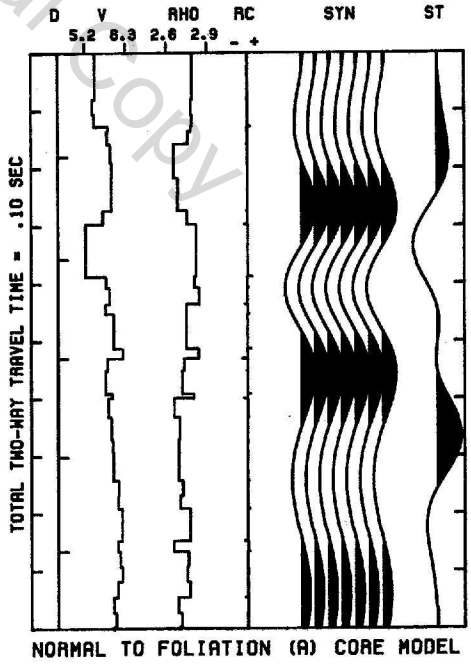

Fig. 14. Reflections originating from a 330-m section of the Brevard fault zone with horizontal foliation. The reflections show the combined effects of anisotropy and chemical variations. For details of plot structure refer to Figure 11 caption and text.

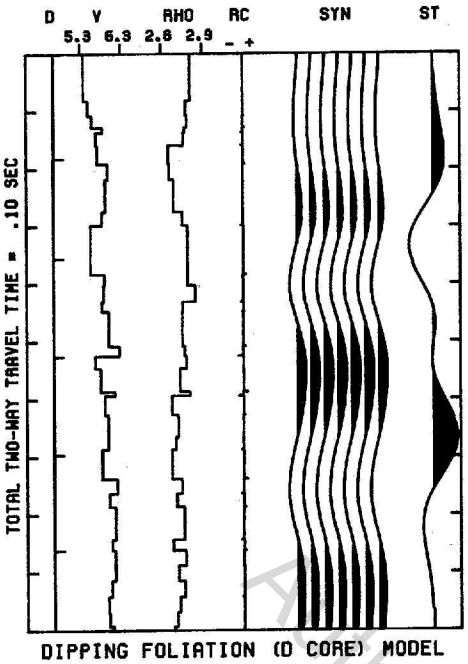

Fig. 15. Reflections originating from a 20°–30° dipping section of the Brevard fault zone. Note the amplitude reduction compared with Figure 14.

variation effects. Velocity normal to foliation in the graphitic phyllonite layer at a depth of 84 m (~0.025 s) is slow (5.21 km s^{-1}), resulting in the large negative reflection event due to anisotropy. However, the low percent SiO_2 produces a relatively high mean velocity for the unit (6.32 km s^{-1}), resulting in a positive reflection event. These effects are partly offsetting, although anisotropy is dominant. The importance of the graphitic phyllonite in producing reflections will depend on the orientation of its fabric, its thickness, and its encasing lithologies. Figure 15 shows the synthetic seismogram for the vertical (D) core data. It is similar to the A core seismogram (Figure 14), but the dipping foliation in the D core samples has reduced velocity contrasts and hence reflection amplitudes. This behavior can be observed in the seismic line of Figure 2, where the Brevard fault zone reflectors increase in amplitude as the dip of the fault zone decreases.

All of the models demonstrate the important effects of interference between reflections from the individual interfaces. The spacing of the interfaces is crucial, as is the frequency of the wavelet. It is probable that strong reflection events from the Brevard fault zone are due to appropriate layering of units of varying density and velocity, such as those described in this paper. Since amplitudes of reflection events are dependent on the spacing of the layers, their chemistry, and their anisotropy, events will grow and die as the geometry and physical properties of the Brevard fault zone lithologies vary laterally. We must emphasize that the models shown here are for a 330-m-length section of core. The actual behavior will depend on the distribution of these lithologies in the remainder of the zone, both laterally and vertically. Figure 16 shows the seismogram for one of myriad possibilities. In this model the actual thicknesses of the units are used, but these are allowed to occur in random vertical order, creating a total thickness of 900 m. This is presumed to be close to the actual total thickness of the fault zone near the Earth's surface. Foliation-normal (A) core velocity-density data pairs are used; these are also distributed randomly over the length of the core. This seismogram, along with many other combinations tried but not shown, demonstrates the highly reflective nature of Brevard fault zone lithologies. The foregoing seismograms indicate the importance of the presence of a variety of lithologies in a fault zone, the variability in the degree of ductile deformation, or both, in producing reflections. Lithologic variations contribute to the chemical variability in the fault zone. Variations in the degree of shearing influences the abundance and degree of orientation of phyllosilicates. A chemically homogeneous fault zone, uniformly sheared throughout, would not be expected to give rise to internal reflections. We believe that these seismic models illustrate important principles for the interpretation of seismic data in crystalline terranes. First, the inherent reflectivity of fault zones has not been fully appreciated. As a consequence, many reflections actually arising from within fault zones have been assigned to the footwall or hanging wall, so that fault zone thicknesses are underestimated. Second, anisotropy and chemical variations may sometimes have offsetting effects, producing seismically transparent regions. This would also contribute to an underestimation of the actual thicknesses of fault zones.

Deep seismic reflection investigations often reveal a marked increase in reflection density in the lower continental crust [e.g., *Meissner*, 1986; *Matthews and Cheadle*, 1986; *Allmendinger et al.*, 1987]. The origin of these reflections, which typically appear to be relatively continuous and cyclic, are problematical. Proposed explanations include cumulate layering [*Meissner*, 1973; *Hale and Thompson*, 1982], intrusive basaltic sills perhaps originating from crustal underplating [*McKenzie*, 1984], subhorizontal zones of fluid-

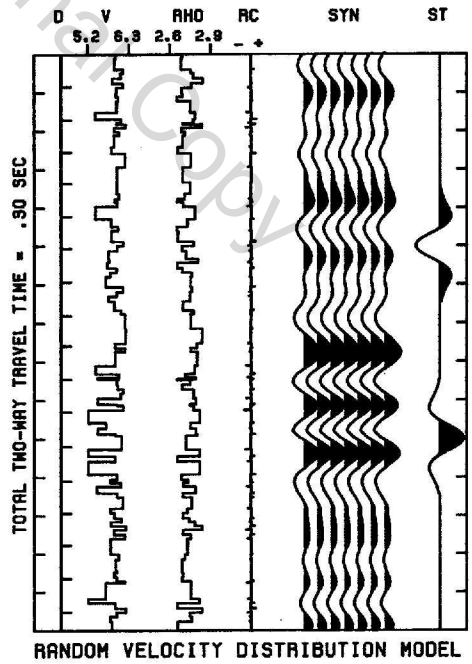

Fig. 16. Seismogram demonstrating the highly reflective nature of a complete section of the Brevard fault zone originating from variability in composition and ductile deformation. Layers consisting of the foliation-normal (A core) velocities and densities of Table 1 are repeated randomly in this section. The vertical scale is compressed to one third of the scale of Figures 11 and 13–15.

filled overpressured cracks [*Matthews and Cheadle*, 1986], and extension or compression, which has produced ductile deformation in the lower crust [*Smithson*, 1986; *Smithson et al.*, 1986]. We believe that the ductile strain origin is the most likely explanation, especially in lower crustal regions characterized by continuous subhorizontal reflections. Reflections from zones of high strain would originate from a combination of (1) the juxtaposition of rocks of different seismic impedances and (2) variations in anisotropy magnitudes, similar to the behavior observed in the Brevard fault zone.

SUMMARY AND CONCLUSIONS

A combination of properties has been found to contribute in a complex manner to the overall reflectivity of the Brevard fault zone. Essential to the study has been the continuous coring of a major section of the Brevard fault zone, which has provided the necessary stratigraphic control as well as unweathered samples for laboratory studies. Velocity measurements, chemical analyses, and synthetic reflection seismograms provide the following conclusions pertaining to the nature of fault zone reflectivity.

1. The Brevard fault zone is not a knife edge fault; rather, it has a thickness at depth, which appears to be borne out in the seismic data. Reflections originate within the Brevard fault zone, not simply at the "top" or "base" of the fault zone where ductilely sheared and unsheared materials are juxtaposed.

2. Anisotropy is a significant seismic property of the Brevard fault zone. Compressional wave velocities are fast parallel to foliation and slow normal to foliation.

3. Preferred orientation of mica associated with ductile deformation is the primary cause of the anisotropy. At low pressures, anisotropy is enhanced by preferred crack orientation. Thus anisotropy usually decreases with increasing pressure.

4. The percentage of anisotropy varies within the Brevard fault zone. This correlates with the amount of mica present and the degree of mica orientation, and is, in part, responsible for reflections from the fault zone.

5. The parent lithologies of the fault zone rocks range in composition from shale to granite. The resulting chemical heterogeneity correlates well with mean compressional wave velocity. This variation of chemistry within the fault zone produces regions of contrasting seismic impedance, which are shown to cause reflections. The chemical variations in the Brevard mylonites, which are not readily apparent in hand sample, are indicators of mean velocities but not of anisotropy effects.

6. Reflections from fault zones within crystalline terranes thus likely originate from a combination of variations of anisotropy and composition. The resulting structural layering within fault zones produces the strong multicyclic reflections. Variations in pore pressure within fault zones are not required to produce the observed reflections.

7. Within fault zones, as we have found in the upper section of the Brevard fault zone drill core, the effects of composition changes, and variations in anisotropy may cancel one another to produce transparent regions. Therefore discontinuity of a fault zone reflector does not necessarily indicate discontinuity of a geologic layer. Estimates of fault zone thicknesses from reflection records should be viewed with caution since they likely represent minimum values.

Acknowledgments. The laboratory studies were supported by the Office of Naval Research contract N-00014-84-K-0207 and a National Science Foundation graduate fellowship to D.L.S. We wish to acknowledge the cooperation of R. D. Hatcher, Jr. and R. T. Williams in providing us with samples of the core which was drilled with funding from the National Science Foundation (grant EAR 8417894). The assistance of C. Wilcox, W. Wepfer, B. Plaskon, D. Ballotti, and D. Kingma is appreciated.

REFERENCES

Allmendinger, R. W., T. A. Hauge, E. C. Hauser, C. J. Potter, S. L. Klemperer, K. D. Nelson, P. Kneupfer, and J. Oliver, Overview of the COCORP 40°N Transect, western United States: The fabric of an orogenic belt, *Geol. Soc. Am. Bull.*, *98*, 308–319, 1987.

Armstrong, R. L., Cordilleran metamorphic core complexes—From Arizona to southern Canada, *Annu. Rev. Earth Planet. Sci.*, *10*, 129–154, 1982.

Birch, F., The velocity of compressional waves in rocks to 10 kilobars, 1, *J. Geophys. Res.*, *65*, 1083–1102, 1960.

Brewer, J. A., D. H. Matthews, M. R. Warner, J. R. Hall, D. K. Smythe, and R. J. Whittington, BIRPS deep seismic reflection studies of the British Caledonides, *Nature*, *305*, 206–210, 1983.

Christensen, N. I., Compressional wave velocities in metamorphic rocks at pressures to 10 kbar, *J. Geophys. Res.*, *70*, 6147–6164, 1965.

Christensen, N. I., Shear wave velocities in metamorphic rocks at pressures to 10 kbar, *J. Geophys. Res.*, *71*, 3549–3556, 1966.

Christensen, N. I., and R. Ramananantoandro, Elastic moduli and anisotropy of dunite to 10 kilobars, *J. Geophys. Res.*, *76*, 4003–4010, 1971.

Clark, H. B., J. K. Costain, and L. Glover, III, Structural and seismic reflection studies of the Brevard ductile deformation zone near Rosman, North Carolina, *Am. J. Sci.*, *278*, 419–441, 1978.

Clarke, F. W., Data of geochemistry, *U.S. Geol. Surv. Bull.*, *770*, 841 pp., 1924.

Cook, F. A., D. S. Albaugh, L. D. Brown, S. Kaufman, J. E. Oliver, and R. D. Hatcher, Jr., Thin-skinned tectonics in the crystalline southern Appalachians: COCORP seismic-reflection profiling of the Blue Ridge and Piedmont, *Geology*, *7*, 563–567, 1979.

Cook, F. A., L. D. Brown, S. Kaufman, and J. E. Oliver, The COCORP seismic reflection traverse across the southern Appalachians, *AAPG Stud. Geol.*, *14*, 61 pp., 1983.

Coruh, C., J. K. Costain, R. D. Hatcher, Jr., T. L. Pratt, R. T. Williams, and R. A. Phinney, Results from regional vibroseis profiling: Appalachian ultradeep core hole site study, *Geophys. J. R. Astron. Soc.*, *89*, 147–155, 1987.

Davis, G. H., Structural characteristics of metamorphic core complexes, southern Arizona, *Mem. Geol. Soc. Am.*, *153*, 35–77, 1980.

Etheridge, M. A., and R. H. Vernon, Comment on "Seismic velocity and anisotropy in mylonites and the reflectivity of deep crustal fault zones," *Geology*, *11*, 487–489, 1983.

Fountain, D. M., C. A. Hurich, and S. B. Smithson, Seismic reflectivity of mylonite zones in the crust, *Geology*, *12*, 195–198, 1984.

Fuchs, K., On the properties of deep crustal reflectors, *Z. Geophys.*, *35*, 133–149, 1969.

Hale, L. D., and G. A. Thompson, The seismic reflection character of the continental Mohorovicic discontinuity, *J. Geophys. Res.*, *87*, 4625–4635, 1982.

Harris, L. D., A. G. Harris, W. De Witt, Jr., and K. C. Bayer, Evaluation of southern Eastern overthrust belt beneath Blue Ridge–Piedmont thrust, *Am. Assoc. Pet. Geol. Bull.*, *65*, 2497–2505, 1981.

Hatcher, R. D., Jr., Stratigraphy, petrology and structure of the Low Rank Belt and part of the Blue Ridge of northwesternmost South Carolina, *Geol. Notes S.C. Geol. Surv.*, *13*, 105–141, 1968.

Hatcher, R. D., Jr., Stratigraphy of the Brevard zone and Poor Mountain area, northwestern South Carolina, *Geol. Soc. Am. Bull.*, *81*, 933–940, 1970.

Hatcher, R. D., Jr., Stratigraphic, petrologic, and structural evi-

dence favoring a thrust solution to the Brevard problem, *Am. J. Sci.*, *270*, 177–202, 1971.

Hatcher, R. D., Jr., Second Penrose Field Conference: The Brevard zone, *Geology*, *3*, 149–152, 1975.

Hatcher, R. D., Jr., Tectonics of the western Piedmont and Blue Ridge, southern Appalachians: Review and speculation, *Am. J. Sci.*, *278*, 276–304, 1978.

Hatcher, R. D., Jr. (Compiler), *Appalachian Ultradeep Core Hole (ADCOH) Project Consortium: DOSECC format preproposal*, 178 pp., University of Tennessee at Knoxville, Knoxville, 1987.

Hatcher, R. D., Jr., J. K. Costain, C. Coruh, R. A. Phinney, and R. T. Williams, Tectonic implications of new Appalachian Ultradeep Core Hole (ADCOH) seismic reflection data from the crystalline southern Appalachians, *Geophys. J. R. Astron. Soc.*, *89*, 157–169, 1987.

Hurich, C. A., S. B. Smithson, D. M. Fountain, and M. C. Humphreys, Seismic evidence of mylonite reflectivity and deep structure in the Kettle dome metamorphic core complex, Washington, *Geology*, *13*, 577–580, 1985.

Jonas, A. I., Structure of the metamorphic belt of the southern Appalachians, *Am. J. Sci.*, *24*, 228–243, 1932.

Jones, T., and A. Nur, Seismic velocity and anisotropy in mylonites and the reflectivity of deep crustal fault zones, *Geology*, *10*, 260–263, 1982.

Jones, T. D., and A. Nur, The nature of seismic reflections from deep crustal fault zones, *J. Geophys. Res.*, *89*, 3153–3171, 1984.

Keith, A., Description of the Mount Mitchell quadrangle (North Carolina–Tennessee), in *Geological Atlas*, folio 124, 10 pp., U.S. Geological Survey, Reston, Va., 1905.

Le Maitre, R. W., The chemical variability of some common igneous rocks, *J. Petrol.*, *17*, 589–637, 1976.

Matthews, D. H., and M. J. Cheadle, Deep reflections from the Caledonides and Variscides west of Britain and comparison with the Himalayas, in *Reflection Seismology: A Global Perspective*, *Geodyn. Ser.*, vol. 13, edited by M. Barazangi and L. Brown, pp. 5–20, AGU, Washington, D.C., 1986.

McCarthy, J., Reflection profiles from the Snake Range metamorphic core complex: a window into the mid-crust, in *Reflection Seismology: The Continental Crust*, *Geodyn. Ser.*, vol. 14, edited by M. Barazangi and L. Brown, pp. 281–292, AGU, Washington, D.C., 1986.

McKenzie, D., A possible mechanism for epeirogenic uplift, *Nature*, *307*, 616–618, 1984.

Meissner, R., The Moho as a transition zone, *Geophys. Surv.*, *1*, 195–216, 1973.

Meissner, R., *The Continental Crust, a Geophysical Approach*, 428 pp., Academic, Orlando, Fla., 1986.

O'Brien, P. N. S., A note on normal incidence reflections from the Mohorovicic discontinuity, *Geophys. J. R. Astron. Soc.*, *9*, 541–545, 1965.

Phinney, R. A., and D. M. Jurdy, Seismic imaging of deep crust, *Geophysics*, *44*, 1637–1660, 1979.

Reed, J. C., Jr., B. Bryant, and W. B. Myers, The Brevard zone: A reinterpretation, in *Studies of Appalachian Geology: Central and Southern*, edited by G. W. Fisher, F. J. Pettijohn, J. C. Reed, Jr., and K. N. Weaver, pp. 261–269, Wiley—Interscience, New York, 1970.

Reif, D. M., and J. P. Robinson, Geophysical, geochemical, and petrographic data and regional correlation from the Arizona state A-1 well, Pinal County, Arizona, *Ariz. Geol. Soc. Dig.*, *13*, 99–109, 1981.

Robinson, E. A., and S. Treitel, The fine structure of the normal incidence synthetic seismogram, *Geophys. J. R. Astron. Soc.*, *53*, 289–309, 1977.

Roper, P. J., and P. S. Justus, Polytectonic evolution of the Brevard zone, *Am. J. Sci.*, *273A*, 105–132, 1973.

Sibson, R. H., Fault rocks and fault mechanisms, *J. Geol. Soc. London*, *133*, 191–213, 1977.

Smithson, S. B., A physical model of the lower crust from North America based on seismic reflection data, The Nature of the Lower Continental Crust, edited by J. B. Dawson, D. A. Carswell, J. Hall and K. H. Wedepohl, *Spec. Publ. Geol. Soc. London*, *24*, 23–24, 1986.

Smithson, S. B., J. A. Brewer, S. Kaufman, J. E. Oliver, and C. A. Hurich, Structure of the Laramide Wind River uplift, Wyoming, from COCORP deep reflection data and from gravity data, *J. Geophys. Res.*, *84*, 5955–5972, 1979.

Smithson, S. B., R. A. Johnson, and C. A. Hurich, Crustal reflections and crustal structure, in *Reflection Seismology: A Global Perspective*, *Geodyn. Ser.*, vol. 13, edited by M. Barazangi and L. Brown, pp. 21–32, AGU, Washington, D.C., 1986.

Williams, R. T., R. D. Hatcher, Jr., C. Coruh, J. K. Costain, M. D. Zoback, R. N. Anderson, J. B. Diebold, and R. A. Phinney, The southern Appalachian ultradeep scientific drill hole: Progress of site location investigations and other recent developments, in *Observation of the Continental Crust through Drilling*, vol. 2, edited by H. J. Behr, F. G. Staley, and H. Vidal, pp. 44–55, Springer-Verlag, New York, 1987.

Wuenschel, P. C., Seismogram synthesis including multiples and transmissions coefficients, *Geophysics*, *25*, 106–129, 1960.

N. I. Christensen and D. L. Szymanski, Department of Earth and Atmospheric Sciences, Purdue University, West Lafayette, IN 47906.

(Received March 16, 1987;
revised September 28, 1987;
accepted October 29, 1987.)